Modeling Fast Pyrolysis of Waste Biomass: Improving Predictive Capability

Frederico G. Fonseca [a], Axel Funke [a]

a: Institute of Catalysis Research and Technology (IKFT), Karlsruhe Institute of Technology (KIT), Eggenstein-Leopoldshaven, Germany

Abstract

This paper addresses the need for versatile models in fast pyrolysis to facilitate the exploration of novel feedstocks and process configurations, minimizing capital and operational expenses. Our model aims to resolve two key challenges: defining a secondary pyrolysis network to align primary pyrolysis products with experimental results, and addressing issues in modeling condensation loops in steady-state, as observed in various fast pyrolysis implementations, including the *bioliq*® I plant, which serves as the basis for this model. The outcomes are promising, revealing minor discrepancies with experimental values in product distribution (1.5%) and condensate composition (6.0%) post-reactor modeling. Further deviations of 3.6% in condensate composition emerge after condenser modeling. Notably, when considering the entire model, discrepancies persist, particularly when applied to biomasses diverging from the calibration material (wheat straw). This research demonstrates the model's efficacy in addressing specific challenges in fast pyrolysis simulation, emphasizing its adaptability to diverse conditions. However, ongoing refinement is essential for enhancing overall predictive accuracy, particularly in scenarios with varying biomass characteristics. The findings contribute valuable insights to the field, paving the way for more robust and adaptable models in the exploration of fast pyrolysis.

Keywords

pyrolysis, waste biomass, simulation, modeling, Aspen Plus®, kinetics

Graphical abstract

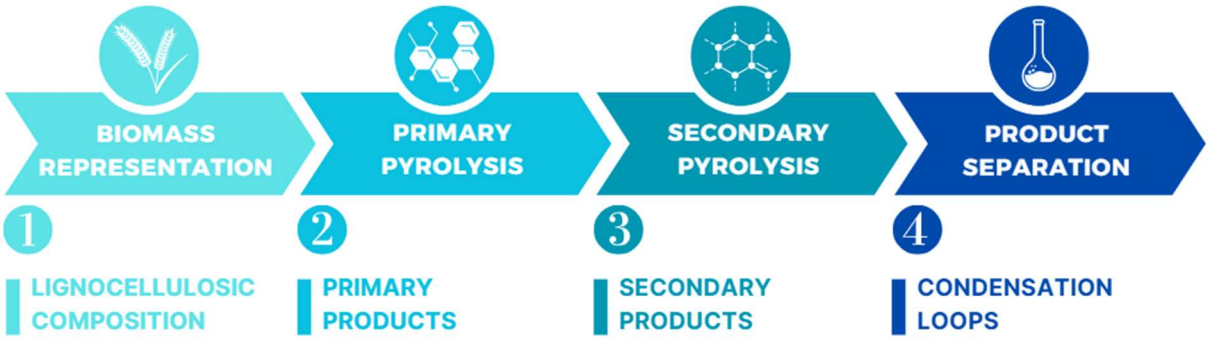

Introduction

Pyrolysis is a thermochemical conversion method of energetic conversion occurring at an inert atmosphere that decomposes macromolecules through the application of heat [1]. When applied to solid biomass, the process yields two main products: a char and a vapor, the latter of which is often condensed to yield one or more liquid phases and a gas phase. To maximize the yield of liquid, fast pyrolysis conditions are often employed, featuring heat heating rates (> 100 °C/s), high temperatures (~500 °C), and short solid and vapor residence times [1–4]. The feedstock's moisture content is also frequently kept low to reduce the water content of the condensates [3], although water is a relevant contributor to the fluidity of the condensates [5].

The composition of the gas product depends on the condensation conditions, and is comprised of gases that do not condensate at normal operation temperatures, like CO, CO_2, light paraffins and any

sweeping gases that may be used throughout the process [1]. Frequently, this gas product is combusted to supply the energy demand of the pyrolysis unit [6,7].

The char retains the vast majority of the inorganic content of the biomass and presents a high heating value [1,8], thus benefiting from a wide range of potential uses. Fluidized bed setups, commonly employed for the processing of biomass in the industry, do not permit the recovery of this material [9].

When considered a single liquid, Fast Pyrolysis Bio-Oil (FPBO) presents a dark-brown color, a viscous buy free-flowing nature and, frequently, a strong smoky odor due to the presence of guaiacols [10]. It has a heating value similar to the feedstock and presents a water content within the range 15-50 wt.% [3,8]. The acidity of FPBO can make it corrosive to some metals and its high oxygen content leads to aging during storage, namely when containing suspended char particles. Despite this, FPBO is primarily used as a fuel for boilers, with limited applications for producing high-value chemicals [11] and potential for upgrade [12] or blending with petroleum fractions [13].

The bioliq® I unit

The *bioliq*® project (www.bioliq.de, [14–16]), initiated in 2007, aims to convert low-grade lignocellulosic biomass into synthetic fuels or organic chemical precursors. Originally using wheat straw, the project expanded to include Miscanthus grass by 2019. Lignocellulosic materials, with low energy density, pose logistical challenges compared to liquid hydrocarbonates. The *bioliq*® concept proposes a decentralized production chain, with biomass thermally liquefied in small-scale units before economic transport to a central plant for gasification and conversion into methanol, DME, and fuels. This decentralization is a key advantage over larger bio-oil production units, due to outsourcing the initial conversion and permitting the use of simultaneous suppliers. The project materialization is located at the Campus North of the Karlsruhe Institute of Technology, Germany.

The model presented in the context of this manuscript focuses on the *bioliq*® I fast pyrolysis plant. This plant is designed for a feed intake of up to 500 kg/h of shredded lignocellulosic material. Utilizing a twin-screw reactor and quartz sand as a heat carrier, the process currently employs a reheating loop making use of natural gas, with a fraction of the produced pyrolysis char being used as an additional heat source, providing precise temperature control. The majority of the coke is removed from the reactor with the vapors and recovered using cyclones. Condensation employs two quenching loop systems in series, yielding two liquid products: an organic-rich condensate (ORC) and aqueous condensate (AC). The two stages differ in the presence on an electrostatic precipitator in the first stage to maximize recovery. Details of the process can be found in [5,17].

Primary pyrolysis networks

Lumped reaction networks that attempt to models the pyrolysis of plant biomass have been developed at least since 2008, with a focus on explicit pathways employing species found in pyrolysis products, but also providing kinetic parameters for each step [21,22].These multicomponent models frequently employ concurrent degradation of lignocellulosic fractions (cellulose, hemicellulose and lignin) and have been found to perform better than single component models at estimating pyrolysis phenomena [23]. However, Carrier et al. [24] reiterate that the identification of chemical reactions based on the conversion of model compounds frequently leads to oversimplified degradation schemes. Moreover, Ward et al. [25] discuss the infeasibility of any reaction model other than black-box systems for processes that involve solid, liquid and gas phases and individual model components, an option also considered by Fonseca et al. [7] and Onarheim et al. [26].

The predecessor to the majority of the reaction networks devised for the modeling of biomass pyrolysis phenomena was published by Ranzi et al. [27] in 2008. The network was developed to

model the pyrolysis of biomass within the context of pyrolysis, and is particularly notorious for representing the entirety of lignin using three monomers, which degrade concurrently but not competitively. The ratio of these monomers in the model can be devised from the H/G/S content of the feedstock [28], or by using error minimization methods to fit the monomers to the elemental composition of the biomass [29]. The original Ranzi model was revised several times, of which noticeable publications include Corbetta et al. [30], Ranzi et al. [31], Ranzi et al. [20,32], Debiagi et al. [33], Corbetta et al. [34] and Anca-Couce and Scharler [35,36]. Trendewicz et al. [37] modified the cellulose part of the degradation network to consider the effect of potassium in the feedstock, by adjusting the energy of activation in order to achieve lower temperatures and faster degradations, compared to the original estimations, proportional to the potassium content in the biomass.

Fonseca et al. [38] examined the ability of various reaction networks at predicting the thermal degradation behavior of two different biomasses, beech wood and wheat straw, while incorporating the effects of potassium content using the Trendewicz [158] modification. All networks performed well when modeling the degradation of beech wood, while not so well when modeling that of wheat straw, mostly due to the high ash content of the latter material. As the Trendewicz model does not consider potassium contents over 1 wt.%, the authors also estimated an optimum value for the potassium content for each reaction network when using wheat straw, thus not requiring further tuning of the model. They found that the Ranzi-Anca-Couce (RAC) [35,36] model performed best overall for both materials, outperforming other models in terms of curve-fit.

Secondary reactions and aging

Secondary pyrolysis is said to happen at any time primary pyrolysis products are held under primary pyrolysis reaction conditions. While this phenomenon is impossible to prevent intra-particle, inter-particle phenomena can be mitigated by maintaning low residence times for both solid and vapor phases in the reactor. This phenomena is exacerbated by the presence of alkali-containing material. [24]

The decomposition of individual pyrolysis bio-oil components has been analysed within vapor-phase pyrolysis. Levoglucosan, the major cellulosic decomposition product, was found to degrade into hydroxymethylfurfural (HMF), glycol aldehyde (HAA), acetol, formic and acetic acids, carbon monoxide, among others [58–61]. HMF can be degradated into furfural through a methylfurfural intermediate step [19,62,63], which forms methylcyclopentenone as a side product [63]. Furfural itself can form furan [64] or vinylketene [65], both instable products. HMF is also known for decomposing into levulinic acid and humins in acid solutions [66]. Levulinic acid itself can degrade over time to form acetic acid and acetone [67]. Xylose/xylosan, form the pyrolysis of hemicellulose, is more labile than its cellulosic equivalent and more readily degrades into HMF, and subsequently to furfural, acetic acid, CO and CO_2 [68–70]. Not as much research has delved into the degradation of lignin intermediaries. As example is sinapaldehyde and p-coumaryl alcohol, common end points of reaction networks, that were isolated and pyrolysed by Herman-Ware et al. [71], and were found to decompose preferentially into syringol (~80 wt.%) and guaiacol (71.4 wt.%) + vanillin (8.1 wt.%), respectively.

Series of secondary gas-phase reactions have been proposed by various authors. Ranzi et al. [27] proposed two series, initiation reactions (25 reactions), and radicular hydrogen abstraction reactions (33 reactions), including several types of components product of the primary pyrolysis reactions. Both of these are designed in the context of pyrolysis as a step for gasification, and thus overestimate the formation of non-condensable gases. Neves et al. [72], Ardila [73] and Peters et al. [29] report using secondary pyrolysis reactions and kinetics for an assortment of sources.

High molecular weight residue

It must be considered that the majority of the reaction networks developed so far are based on thermogravimetric and Py-GC/MS data, therefore do not consider the formation of a hydrophobic high molecular weight residue (also known as 'pyrolytic lignin') such as the one comprising a large fraction (15-30 wt.% db.) of most pyrolysis bio-oils [47]. Peters et al. [29] found a large discrepancy between experimental and estimated values. The nature of this high molecular residue is a currently underexplored subject, as it cannot be analyzed using ubiquitous techniques like GC/MS, but lignins from different provenience have been evaluated by means of a mix of techniques [28,48,49]. Disregarding this fraction reduces the rigorousness of the model and indubitably influences the behavior of liquid-vapor separation estimations [6,7,50,51].

Several authors proposed identities for this phase, while several just defined the high molecular weight residue as a pseudo-component of null vapor pressure [26]. Elliott et al. [52] proposed a molecular weight range of 1000-2500 $g \cdot mol^{-1}$, while Scholze et al. [28] propose a range of 684-692 $g \cdot mol^{-1}$. Ranzi et al. [20,32] and Gorensek et al. [44] propose a single molecule with a molecular weight of 380.5 $g \cdot mol^{-1}$ ($C_{24}H_{28}O_4$), on a lower range, while Ille et al. [53] [53]proposes a surrogate with a molecular weight of 202.2 $g \cdot mol^{-1}$ ($C_{12}H_{10}O_3$), suitable for liquid-vapor modeling. Manríque et al. proposed diverse structures of dimers, trimers and tetramers with a molecular weight range of 326.7-758.3 $g \cdot mol^{-1}$. Fonseca [91] developed a surrogate based on the results presented by Scholze et al. [28] with a molecular weight of 680.2 $g \cdot mol^{-1}$.

It must be kept in mind, that the high molecular weight residue of lignocellulosic bio-oils is not solely derived from lignin. Fortin et al. [54] report the presence of carbohydrate contaminants bonded through ester links. Pires et al. [55] and Fonts et al. [56] make use of both humins (condensed sugars) and hybrid oligomers alongside a pyrolytic lignin to represent the totality of the high molecular weight residue.

The decision on the representation of this phase requires an equilibrium to be stricken between thermodynamic modeling and a lignin-like structure. However, Kröhl [53,57] has shown that less complex surrogates tend to perform better during thermodynamic modeling, to the determent of being worse structural models for the real material.

Modeling of pyrolysis systems using Aspen Plus®

Flowsheeting program packages are very suitable for the design and simulation of processes. Software like this uses unit block abstractions to model real equipment, while providing the user with the parameters and thermodynamic consistency required to produce realistic results. Aspen Plus®, the software of choice in this case, was chosen due to its relative ease of use, as well as ubiquity in both academia and industry. The Aspen Simulator® package also includes the powerful Aspen Properties® database, which includes not only an enormous variety of chemical species but also the ability to estimate *in-situ* (and during simulation) properties based on structural and group contribution methods.

Aspen Plus® has already been the software of choice for the modeling of diverse pyrolysis processes, at different levels of complexity. In Table 1, one can find a compilation of these models, as well as providing insights into the solutions devised to model the reactor and product recovery. As it can be seen, a very common solution is Gibbs minimization [39–41], which features an obvious downgrade of being unfeasible to predict the composition of the condensates [41]. Another alternative is the implementation of reaction networks, such as the ones evaluated by Fonseca et al. [38], also successfully implemented by different authors [23,29,42]. Black box systems and stoichiometric reactors feature the obvious upside of being easy to setup based on experimental data, but do not allow for the prediction of different system behaviors at different operating conditions.

All setups, except black-box reaction models, employed an initial step that converts the solid biomass into its elemental composition or into the lignocellulosic components. Peters et al. [29] reinforced the lack of data available for the modeling of the latter components, especially when using multiple lignin representatives, and partially employed the findings by Wooley and Putsche [43] to bridge this gap. Several years later, Gorensek et al. [44] provided a consistent characterization to all lignin representatives, including thermophysical properties.

Table 1: Summary of models developed in Aspen Plus® for the modeling of biomass pyrolysis, highlighting the reactor configuration and the types of product recovery.

Reference	Process	Reactor	Product recovery	HMW Residue
Demol et al. [45]	Autothermal pyrolysis	Coupled with ANSYS CHEMKIN® Pro 17.0 to model reactor conditions	Flash condenser Removal of coke	No
Fonseca et al. [7]	Fast pyrolysis of wheat straw at different moisture contents	Black box	Flash condenser Removal of coke	No
Hammer et al. [46]	Fast pyrolysis of equine waste	Stoichiometric reactor with gas combustion	Flash condenser with recirculation of gas Removal of coke	No
Humbird et al. [23]	Entrained-flow fast pyrolysis of softwood, cornstover and switchgrass	Custom equation-oriented model employing reaction kinetics. Uses product gas as fluidizing medium	Quench loop condensation with scrubber modeled as rigorous column Integrated coke combustion	No
Kabir et al. [39]	Pyrolysis of municipal green waste	1. Black box for biomass elemental decomposition 2. Gibbs minimization reactor	Integrated combustion of gas and coke Flash condenser	No
Lestinsky et al. [40]	Pyrolysis of spruce sawdust	1. Black box for biomass elemental decomposition 2. Gibbs minimization reactor	Flash condenser Removal of char with inert heat carrier	No
Mohammed et al. [42]	Fast pyrolysis of Napier grass bagasse integrated in biorefinery	1. Fluidized bed unit block for defining fluid dynamics and drying using product gas as fluidizing medium 2. Black box for biomass elemental decomposition 3. CSTR	Integrated coke combustion Flash condenser	No
Onarheim et al. [26]	Fast pyrolysis of pine wood and forest residue	Black box	Integrated combustion of gas and coke Scrubber condenser modeled as rigorous column	Yes, pseudocomponent “null vapor pressure”

Peters et al. [29]	Fast pyrolysis of beech wood	1. Black box for biomass elemental decomposition 2. CSTR 3. Black box for secondary pyrolysis adjusting based on alkali content on biomass	Removal of coke Quench loop condensation with scrubber modeled as flash unit	No
Visconti et al. [41]	General study of pyrolysis of biomass	1. Black box for biomass elemental decomposition 2. Gibbs minimization reactor	Flash condenser Removal of coke	No

Condensation systems used for pyrolysis at middle-large scales are often based on large temperature shocks, like quenching systems using cold fluids (frequently cooled down pyrolysis condensate). Operation of these systems requires the reservation of a start-up time before steady-state can be assumed to be achieved, as the loops must be initialized with entrainers or cooling fluids. Unfortunately, there is a lack of solutions for these topics discussed in the literature [81], and the systems are frequently simplified into abstractions modeling vapor-liquid flash distillation, or using rigorous scrubber columns that may be hard to converge during simulation, and which modeling details are frequently not reported in the literature [23,26,46], as can be seen in Table 1. No details about the number of stages and characteristics of the column models have been found in the literature, though.

Objectives

This manuscript concerns itself with the modeling of a fast pyrolysis unit using Aspen Plus™. Particular attention is given to the decision of reaction network as a follow-up to the work presented in [38], to the definition of secondary pyrolysis reactions and dealing with the presence of aging phenomena. The modeling of looping condensation systems is also heavily discussed, and strategies are compared.

Methodology

The model comprises a complete description of the *bioliq®* I plant, based on campaign data from the years 2015-2018. Modeling was done in Aspen Plus® V14, and makes use of separate hierarchies, which are blocks that contain models within themselves, and communicate with the greater model only by material, heat or work streams; this presents an obvious advantage for sequential modeling, and also permits the isolation of fractions of the model for troubleshooting.

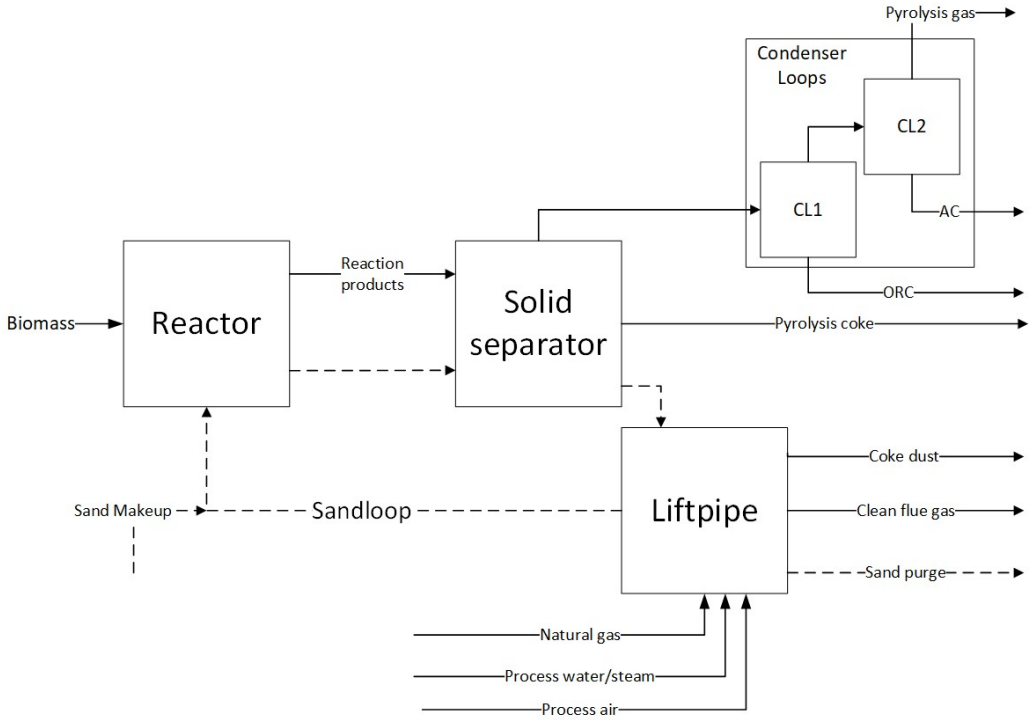

Figure 1: Scheme of the model flowsheet, evidencing the different hierarchies (squares) and their inputs/outputs.

A scheme of the model can be seen in Figure 1. The condensation systems were kept in a single hierarchy, separated as two sub-hierarchies, to facilitate any potential future customization of the model. The detailed description of the unit blocks and their placement can be found in the Supplementary Information.

[14–16][5,17]Modeling of the reactor

During the modeling of the reactor the sand loop was kept separate from the reaction blocks to facilitate convergence. The modeling of the reactors is, thus, performed assuming a similar logic than the one proposed by Peters et al. [29]. A first step employs a black-box reactor, which splits the biomass into its lignocellulosic components, the second step employs a primary pyrolysis reactor, and the third considers secondary pyrolysis and delayed volatilization of coke, a phenomenon present in all considered reaction network variants. The characteristics of the feedstocks can be found in Table S 1 in the SI.

Primary reactor

As seen in Table 1, kinetic models have proven to provide good estimations of product distribution after pyrolysis, without featuring the downsides of Gibbs minimization models or black box abstractions. Among kinetic models, without requiring custom modeling or coupling with external software, the options to consider are stirred-tank models (CSTR), characterized by the volume or by the residence time of the fluid, and plug-flow models (PFR), characterized by the dimensions of the tube(s). Henrich et al. [82] claim that PFR models are a good fit when modeling the *bioliq®* pyrolysis

reactor, but these models present frequent convergence issues and mass balance errors, especially when employing complex reaction networks and the presence of multiple phases. On the other hand, several researchers have successfully employed CSTR models when employing complex reaction networks [29,42].

[29]The thermodynamic model employed is Peng-Robinson with Quadratic Huron-Vidal-Michelsen mixing rule (PRMHV2), in line with other publications employing Peng-Robinson variants while modeling pyrolysis processes with Aspen Plus™ [29,44].

The calculations assumes a feedstock input of 360 $kg \cdot h^{-1}$, characterized as a non-conventional solid. Non-conventional solids are characterized by their proximate and ultimate analysis. Enthalpy of formation is estimated based on the heat of combustion, provided for each biomass. Heat capacity and density are estimated based on the ultimate analysis (HCOALGEN and DOALIGT, respectively) [83].

The heat carrier is modeled at silicon dioxide (SiO_2). It is supplied at 556 °C based on *bioliq*® campaign data, at a fixed flow rate of 14.4×360 $kg \cdot h^{-1}$. The heat demand of the process is difficult to estimate, and several ranges are proposed for the pyrolysis process. Polin et al. [84] propose a range of 0.75-1.75 $MJ \cdot kg^{-1}$ for woody biomasses, while Zheng et al. [85] reached a range of 1.16-3.06 $MJ \cdot kg^{-1}$ for wheat straw in the context of an LCA analysis. Yang et al. [86] proposed a methodology based on the heat potential of the products, from which we can calculate the value of 1.10 $MJ \cdot kg^{-1}$. Henrich et al. [82] estimated the specific energetic demand of a similar reactor as 1.25 $MJ \cdot kg^{-1}$ before accounting for the moisture content of biomass, corresponding to a value of 1.45 $MJ \cdot kg^{-1}$ (assuming wheat straw). Based on campaign data, the heat drop for the heat carrier is estimated at 49 °C, dealing to an expected reactor heat demand of 56.4 kW, equivalent to a specific heat demand of 0.56 $MJ \cdot kg^{-1}$, around a third of the value expected by Henrich et al. [82].

The reactor presents a total length of 2030 mm, and the screws present a total length of 1780 nm, of which the first 234 nm correspond to the conveying of the biomass, thus the reaction length can be assumed as 1546 mm. The screws present a pitch of 378 mm and diameter of 190 mm, and in normal operation rotate at 2 Hz. Based on these values, it is possible to estimate the rotation and Froude numbers of the reactor, at 4.1 and 1.53, respectfully.

While the reactor dimensions are known, the residence times of either solid or vapor phases are not. Grandl [87] proposes a value of 10.16 s for the solid residence time, while a value of 1.5 s is assumed for the vapor residence time, estimated based on the typical sweeping gas flow rate. Peters [88] estimated the efficiency of the transport process in auger reactors, and concluded it could be expressed as function of the Froude number of the system, corresponding to a value of 17.71% assuming an angle of 20° and a pitch tangent of 0.745. Based on the rotation number and the frequency and the estimated efficiency, this corresponds to a residence time of 11.55 s, and thus a reactor diameter of 106 mm when the heat carrier is considered, or 27 mm when not.

Simulations were performed using Aspen Plus™, using the best results reported by Fonseca et al. [38], contrasting CSTR and PFR models. The presence of the heat carrier was disregarded; thus, the heat demand was estimated to match with the expected experimental value (56.4 kW). The mass balance closure was also reported, due to the stoichiometric unbalancing present in the reaction networks present in the literature. Not only the deviation in the product distribution (vs. experimental balance results) but also that in the fraction of condensable bio-oil associated compounds. Finally, the results reported by Fonseca et al. [38] for the deviation of derivative fit of each model are also presented here. All of these values are reported in Table 2.

Secondary reactor

Secondary pyrolysis reactions are essential to the correct modeling of a fast pyrolysis process, especially when the bio-oil and its characteristics are important parameters. However, as mentioned in the introduction, secondary pyrolysis is a topic for which fully characterized reactions with kinetics are mostly unavailable, save the work by Ranzi et al. [27], which over estimates the vapor product. Other authors dealing with process simulation, who also employed reaction networks, did solve this issue by frequently gathering reaction formulas and balances and kinetics from different sources.

The selection of a secondary pyrolysis network should carefully account for the composition of the primary pyrolysis product. It is crucial for any secondary pyrolysis network to rectify the disparity between the product distribution and composition of primary pyrolysis reaction products and experimental bio-oil characterization data. Several significant phenomena contribute to this discrepancy, including:

- Degradation of intermediaries, such as p-coumaryl alcohol and sinapaldehyde, which are end products of primary pyrolysis networks but are often absent from final analyses [71];
- Degradation of excess levoglucosan, xylose, HMF and others [63] [58–61] [62];
- Complete decomposition of labile intermediaries like glyoxal and linoleic acid [27] [89,90]

The development of a secondary pyrolysis network must also consider the formation of high molecular weight residue (HMWR). The identity of this product is crucial, as it can arise directly from the degradation of lignin intermediaries and furans, or through long-term storage processes involving oxygenate condensation. In this work, the HMWR was modeled based on analyses and molecular weight ranges reported by Scholze et al. [28], as developed by Fonseca [91].

Several of these phenomena were studied under conditions significantly different from those encountered during fast pyrolysis. Moreover, kinetic data for these phenomena are often lacking, necessitating the adoption of kinetics derived from generalized secondary pyrolysis studies. In some cases, adjustments were made to these kinetics to better align with the actual operating conditions. The complete network can be found in Table S 7 of the Supplementary Information.

Modeling of the condensation loops

Quenching is an effective measure to condense hot pyrolysis gases, by contacting them with a relatively high flow of cooled liquid. A cost-efficient quenching medium avoids downstream decantation and the introduction of external materials. In the case of the bioliq® process, the system operates in transient state employing ethylene glycol as start-up material (water for the second condensation loop), which is replaced overtime by condensate, removing any non-condensed vapors using a scrubbing column after quench. The process also employs an electrostatic precipitator to ensure the total recovery of liquid droplets that may have been entrained in the outgoing vapors.

Modeling of such loops in steady-state is difficult. While the presence of the electrostatic precipitator can be disregarded, the modeling of a scrubbing column is often done by trial-and-error and depends heavily on the nature of the incoming streams, as no heat is introduced or removed from the system to ensure operation. Moreover, as the flowrate of looping liquid material is much higher than the incoming and outgoing stream, it is important to ensure that the initial state of the recirculating material is defined to a way that will ensure convergence without affecting the composition of the bio-oil significantly.

Modeling these systems in a steady-state system can be difficult, as three constrains must be defined *a priori*: 1. The flowrate of the hot gas entering the loop; 2. The flowrate of either liquid and vapor exits, which can be defined by roughly estimating the volatility of the condensate at condensation conditions assuming heavy and light key components; 3. The initialization of (at least one) looping

tear stream, which flowrate is often higher than both input and output streams, which composition must be close enough to the target to ensure convergence, but not too close that it may not vary with a different input composition.

The modeling of the scrubbing columns does not follow any specific guidelines and must be made using trial-and-error to produce reasonable approximations to experimental results. Estimation of the flowrate of liquid condensate for each case was done by defining a flash distillation unit in which the incoming gases are separated at experimental process conditions, and forcing the desired flowrate to equal that of the flash liquids.

The thermodynamic property method employed is Soave-Redlich-Kwong with the Kabadi-Danner mixing rule (SRK-KD) following the results presented by Fonseca [91]. This method presented the lowest deviations in a model and mixture similar to the one presented in this work, using the same HMWR.

Several strategies can be used to define the initial conditions of the recirculating material. Fonseca [91] contrasted four initialization cases for which the deviations (ε) were estimated for the case of wheat straw as feedstock:

- Case 1: loop is initialized using the start-up material, leading to a product of low value;
- Case 2: simplified mixture consisting of five components (water, acetic acid, acetol, levoglucosan, HMWR);
- Case 3: average of bio-oil compositions of different feedstocks;
- Case 4: complex mixture consisting of 15 components

In the context of this work, a 5^{th} case is considered:

- Case 5: simplified mixture consisting of 4 LVE components and 3 solid coke components over 5 wt.%, plus a FORTRAN routine equating the mass fraction of components in the tear stream (> 1 wt.%) used for initialization with those obtained in the flash.

Results and discussion

Primary pyrolysis

Based on the data reported in Table 2, similarly low product distribution deviations were found for the Ranzi 08 [27] + Trendewicz [37] – Exp model, the RAC [36] + Trendewicz [37] – Opt model and the RAC [36] + Trendewicz [37] - Exp, using CSTR models. The lowest condensate composition deviations were found for the Ranzi 17 [32] + Trendewicz [37] – Opt, which did not present such a good value for the product distribution; however, both RAC-Exp and RAC opt models performed appreciably in this situation. Between the latter, the Opt presents a much better performance at modeling the biomass degradation, while presenting a reasonable mass balance deviation, and a high heat demand.

On a second series of tests, variants of the best performant cases of Table 2, Ranzi 08 [27] + Trendewicz [37] – Exp and RAC [36] + Trendewicz [37] – Opt. were contrasted. The variants consider the use of the kinetic parameters determined by Fonseca et al. [38] and alternative hemicellulose degradation pathways (production of xylosan vs low molecular weight compounds), contrasting hardwoods and grasses by Debiagi et al. [33]. The results are presented in Table 3. Here, a similar analysis as the one made for Table 2 can be easily made. The main focus being the deviation of the product distribution and the secondary focus being the deviation of the condensate composition. Several variants of both base cases present similarly low deviations, mostly using CSTR models, but the base RAC [36] + Trendewicz [37] – Opt without any modifications presented the best results.

Table 2: Results of simulations performed using the different reaction networks. CSTR assumed a residence time of 11.55 s, PFR assumed dimensions of 1546×27 mm. Coke volatilization reactions performed using CSTR models assuming a residence time of 1.5 s. Tests performed assuming wheat straw.

		CSTR					PFR				
	Potassium content (wt.%)	Deviation of model	Heat Demand (kW)	Error of mass balance	Deviation of derivative fit [38]	Deviation of condensate composition	Deviation of model	Heat Demand (kW)	Error of mass balance	Deviation of derivative fit [38]	Deviation of condensate composition
Ranzi 08 [27]	0.00	11.7%±3.5%	88.5	1.2%	21.5%	23.5%±2.0%	11.0%±1.6%	80.1	1.0%	21.5%	24.9%±2.0%
Ranzi 08 [27] + Trendewicz [37] - Exp	1.18	5.3%±2.1%	80.3	1.3%	34.1%	21.3%±2.1%	5.5%±1.2%	73.1	1.3%	34.1%	23.2%±2.1%
Ranzi 08 [27] + Trendewicz [37] - Opt	0.07	8.1%±2.8%	90.5	1.3%	15.7%	21.6%±2.0%	8.1%±1.1%	82.8	1.2%	15.7%	23.1%±1.9%
Corbetta [30]	0.00	9.8%±2.9%	228.8	4.3%	20.6%	24.3%±1.8%	15.3%±2.3%	84.5	0.6%	20.6%	25.1%±1.7%
Corbetta [30] + Trendewicz [37] - Exp	1.18	6.0%±2.4%	224.1	4.3%	26.7%	23.3%±2.2%	10.7%±1.6%	92.6	0.7%	26.7%	24.3%±2.2%
Corbetta [30] + Trendewicz [37] - Opt	0.09	8.4%±2.5%	229.3	4.3%	12.8%	23.6%±1.9%	13.2%±0.9%	98.4	0.6%	12.8%	24.4%±1.8%
RAC [36]	0.00	11.4%±3.2%	115.4	4.0%	25.2%	20.3%±1.7%	12.6%±0.6%	87.5	3.9%	25.2%	21.2%±1.8%
RAC [36] + Trendewicz [37] - Exp	1.18	5.8%±2.6%	109.0	4.0%	28.1%	15.9%±2.0%	6.8%±1.2%	87.4	4.0%	28.1%	18.9%±2.0%
RAC [36] + Trendewicz [37] - Opt	0.39	5.5%±2.4%	109.8	4.0%	10.7%	16.8%±1.9%	8.5%±0.8%	88.9	3.9%	10.7%	19.8%±1.9%
Ranzi 17 [32]	0.00	10.7%±3.1%	169.0	0.4%	26.1%	24.1%±1.6%	12.8%±0.4%	124.8	3.6%	26.1%	25.4%±1.7%
Ranzi 17 [32] + Trendewicz [37] - Exp	1.18	10.8%±3.6%	167.7	0.5%	34.8%	15.2%±2.1%	8.6%±2.0%	136.3	0.3%	34.8%	18.2%±2.0%
Ranzi 17 [32] + Trendewicz [37] - Opt	0.12	7.4%±4.1%	169.6	0.5%	13.8%	13.6%±2.2%	8.3%±2.2%	118.8	5.1%	13.8%	18.4%±2.0%

Table 3: Results of simulations performed using variations of Ranzi 08 [27] *+ Trendewicz* [37] *– Exp and RAC* [36] *+ Trendewicz* [37] *- Opt. CSTR assumed a residence time of 11.55 s, PFR assumed dimensions of 1546×27 mm. Coke volatilization reactions performed using CSTR models assuming a residence time of 1.5 s. Tests performed assuming wheat straw.*

			CSTR				PFR			
	Debiagi [33]	Experimental Kinetic Parameters [38]	Deviation of model	Heat demand (kW)	Error of mass balance	Deviation of Condensate composition	Deviation of model	Heat demand (kW)	Error of mass balance	Deviation of condensate composition

R08-Exp	Original	-	5.3%±2.1%	80.3	1.3%	21.3%±2.1%	5.5%±1.2%	73.1	1.3%	23.2%±2.1%
	Original	KAS	9.8%±2.9%	97.3	1.3%	17.1%±1.9%	9.1%±1.4%	91.6	1.4%	23.2%±2.2%
	Original	Curve-Fit	8.4%±2.8%	93.8	1.3%	22.2%±2.2%	8.7%±0.9%	83.7	1.1%	23.7%±2.2%
	Cereal	-	5.3%±2.1%	84.4	0.8%	21.6%±2.1%	6.1%±1.3%	76.2	0.9%	23.8%±2.1%
	Cereal	KAS	9.7%±3.1%	101.4	0.8%	22.4%±2.2%	9.8%±1.1%	93.8	0.8%	23.7%±2.2%
	Cereal	Curve-Fit	8.6%±2.7%	98.2	0.8%	22.4%±2.2%	10.4%±0.5%	88.1	0.8%	23.9%±2.2%
	Hardwood	-	5.3%±2.1%	81.0	1.2%	21.4%±2.1%	5.5%±1.2%	71.9	0.9%	23.4%±2.1%
	Hardwood	KAS	9.8%±2.9%	98.0	1.2%	22.3%±2.2%	9.2%±1.3%	92.2	1.3%	23.3%±2.2%
	Hardwood	Curve-Fit	8.3%±2.8%	94.6	1.2%	22.2%±2.2%	8.9%±0.8%	85.0	1.2%	23.8%±2.2%
RAC-Opt	Original	-	5.5%±2.4%	109.8	4.0%	16.8%±1.9%	8.5%±0.8%	88.9	3.9%	19.8%±1.9%
	Original	KAS	13.8%±1.0%	99.0	0.1%	21.9%±2.1%	14.9%±1.1%	84.7	0.4%	23.5%±2.1%
	Original	Curve-Fit	13.1%±1.5%	92.8	0.1%	22.6%±2.1%	14.4%±1.3%	71.8	1.9%	24.5%±2.2%
	Cereal	-	5.3%±2.2%	107.9	4.0%	17.5%±2.0%	9.7%±1.1%	74.6	3.9%	20.2%±2.0%
	Cereal	KAS	13.8%±1.0%	99.0	0.1%	21.9%±2.1%	14.9%±1.1%	84.7	0.4%	23.5%±2.1%
	Cereal	Curve-Fit	13.2%±1.2%	98.5	0.1%	21.8%±2.1%	14.5%±1.1%	74.5	2.7%	23.5%±2.1%
	Hardwood	-	5.3%±2.3%	108.6	4.0%	16.9%±2.0%	9.1%±0.9%	85.3	3.9%	19.6%±2.0%
	Hardwood	KAS	13.8%±1.0%	99.0	0.1%	21.9%±2.1%	14.9%±1.1%	84.7	0.4%	23.5%±2.1%
	Hardwood	Curve-Fit	13.2%±1.2%	109.8	4.0%	16.8%±1.9%	8.5%±0.8%	88.9	3.9%	19.8%±1.9%

Secondary pyrolysis

Both product distribution and bio-oil composition are contrasted with the experimental results and the results of the best performant primary pyrolysis network, and the results are shown in [27][71][63][58–61][62][27][89,90][28][91]Figure 2.

It must be kept in mind that this composition is done before any condensation systems are considered. The components of the organic liquid yield are all non-water condensable species present in the mixture.

The results after including the secondary pyrolysis stage present large improvements when compared to the primary pyrolysis results, thus exacerbating the importance of considering the presence of these phenomena during modelling. Deviations from experimental data improved from 6.6 to 1.5% for the product distribution, and from 10.6% to 6.0% for the bio-oil composition, the latter still presenting clear outliers in the aldehyde, HMWR and water contents.

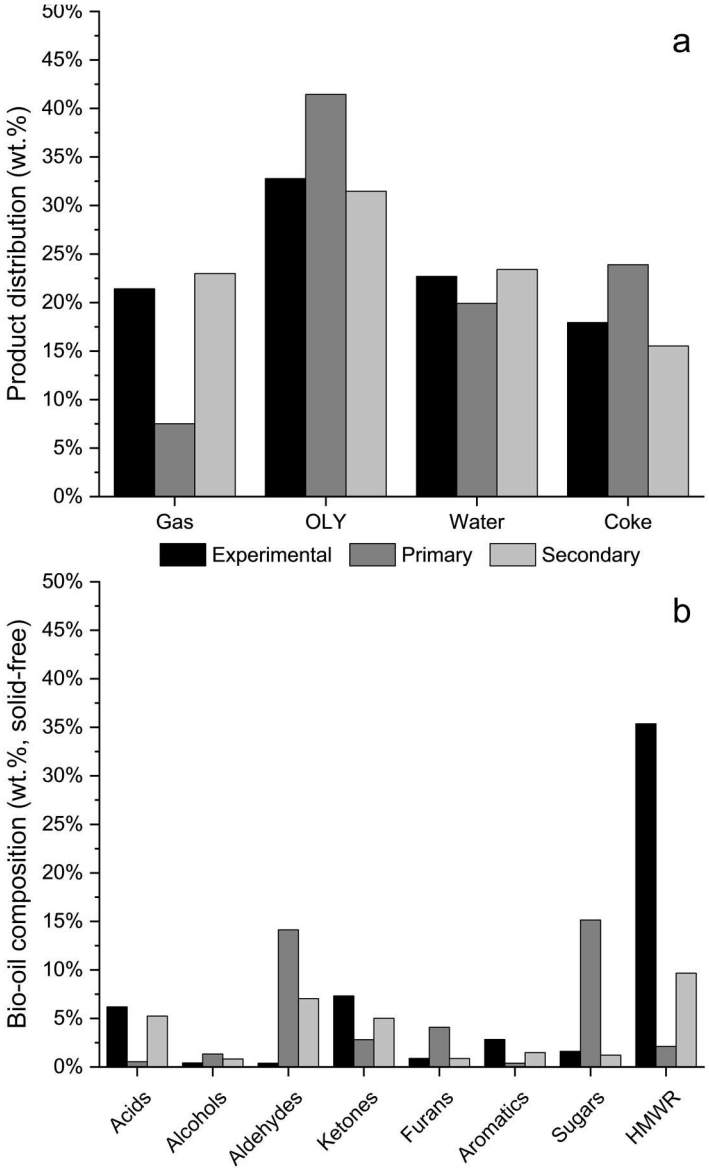

Figure 2: Simulation results after secondary pyrolysis, contrasted with primary pyrolysis and experimental results. a: Product distribution; b: Bio-oil composition assuming all possible condensable species. Experimental data sourced from bioliq® campaigns between 2015 and 2018. OLY: Organic liquid yield. Coke is reported ash-free.

Modeling of the condensation loops

While the results of the secondary pyrolysis of may indicate a good approximation of experimental results, it is expected that a fraction of the organic condensates and the water in the system will be removed in the gas phase.

The definition of the initial conditions of the recirculating material has produced different results depending on the case described in the Methodology. Deviations from experimental results in terms of the composition of the condensate for each case are the following:

- Case 1: 165 wt.%
- Case 2: 48 wt.%
- Case 3: 47 wt.%
- Case 4: 41 wt.%
- Case 5: 4 wt.%

Due to the significant difference in the flow rate of the quenching material compared to the incoming vapor, there will likely be substantial variations in the results. In contrast to all other cases, where only a group of substances are chosen beforehand to initialize the loop, case 5 can vary the composition of the initialization based on the material incoming from the reactor.

Case 5 differs in the fast that the mass fractions of the liquid phase of the test flash unit are used to initialize the quenching material. When examining the results from Figure *3*, which were generated using case 5, it becomes apparent that there is a notable disparity between the predicted and actual values for the recovery of all substances other than sugars and HMWR, due to overestimated volatility at process conditions. This indicates relevant shortcomings of the thermodynamic model and the use of flash models as a first approach to the model.[91]

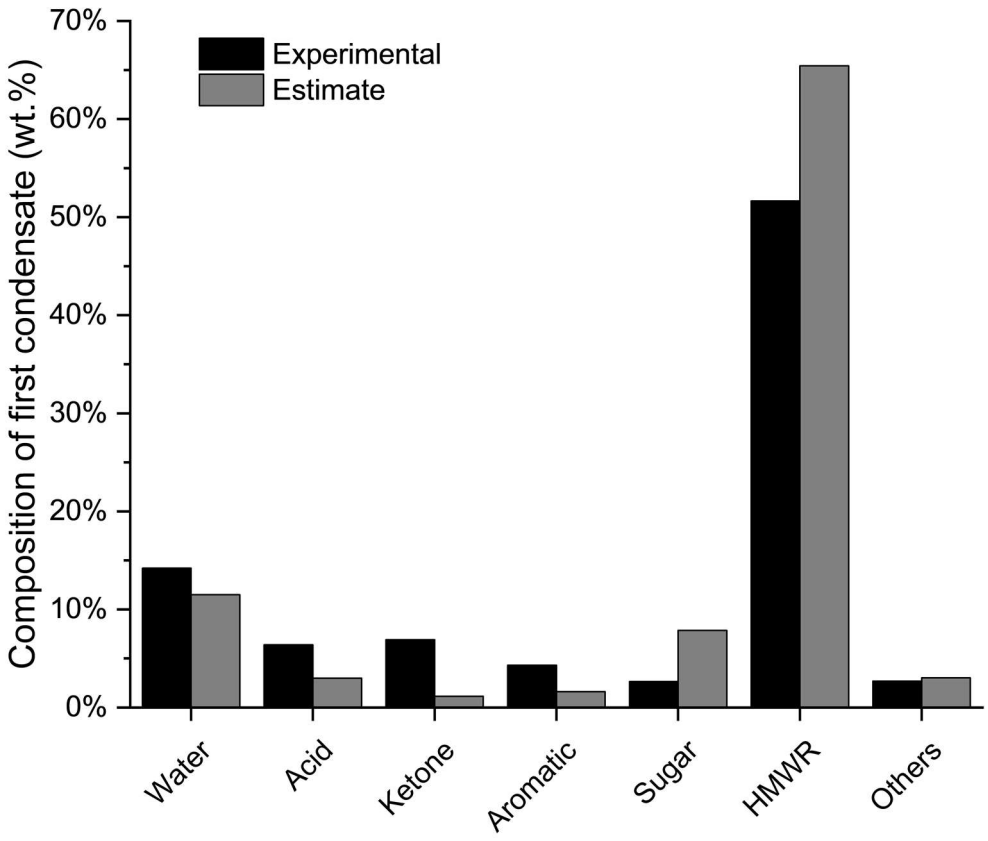

Figure 3: Comparison of estimated composition of condensate with experimental values for case 5. Experimental data sourced from bioliq® campaigns between 2015 and 2018.

Model validation

The model was developed using wheat straw as the calibration biomass, and its validation will be done making use of four different feedstocks for which experimental data is available in our internal database: wheat straw, *Miscanthus* grass, sugar cane bagasse and beech wood. The results can be found in Figure 4.

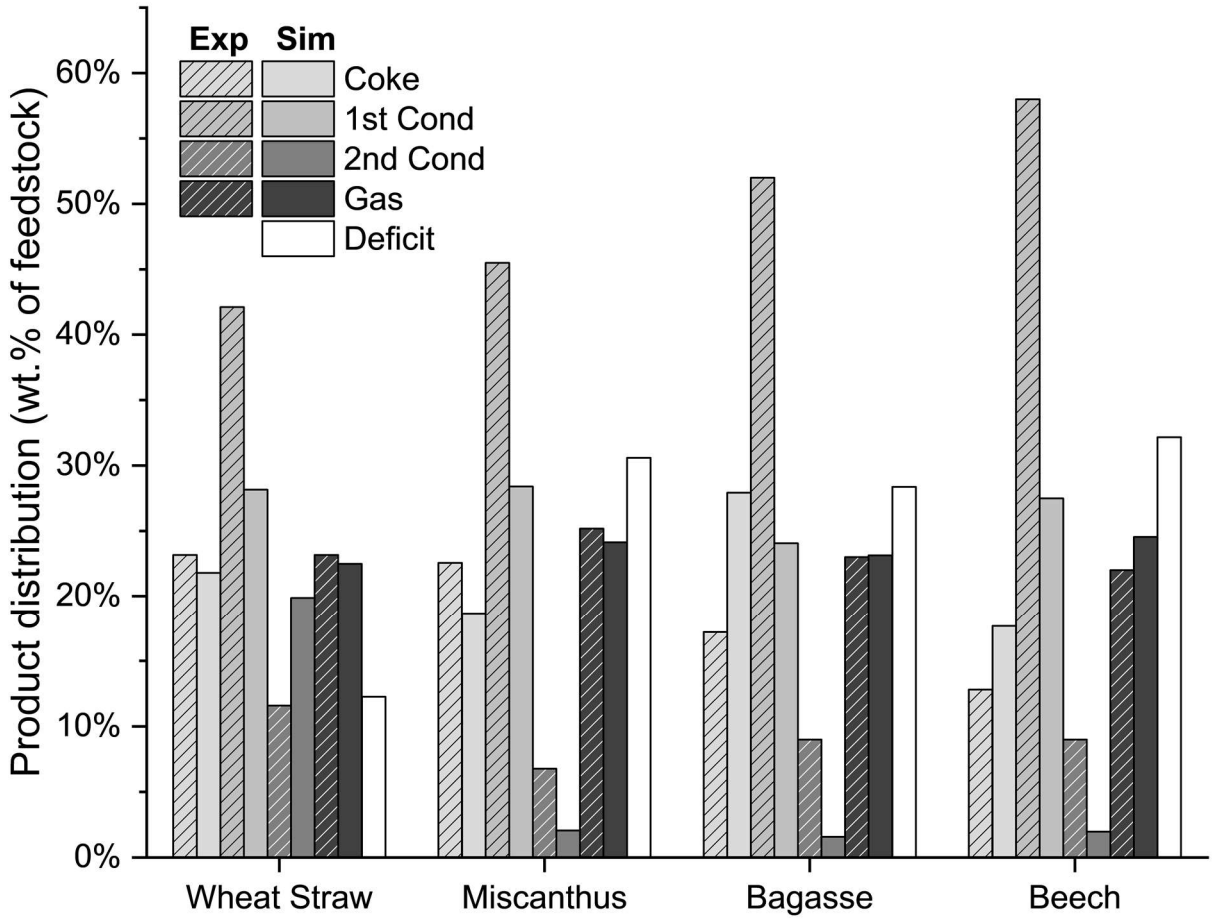

Figure 4: Comparison of product distribution between experimental and simulated results. Experimental data sourced from the internal database in IKFT-KIT. Deficit calculated assuming a difference to 360 kg/h.

As observable in Figure 4, there are noticeable deviations for all biomasses. It is important to keep in mind that while the feed characteristics were changed between each feedstock, including the lignocellulosic distribution, the remaining characteristics of the model were left unaltered.

Average deviations to the experimental base based on the product distribution were the lowest for wheat straw (6.1 wt.%), followed by *Miscanthus* (6.2 wt.%), bagasse and beech (11.6 wt.%, 11.2 wt.%). The low differences between the first two feedstocks can be explained by a similar characterization (Table S 1 in the SI), while the remaining two deviate further in either ash or moisture contents, while the differences in lignocellulosic analysis is not high enough to come into more clear conclusions.

For all feedstocks, relevant discrepancies are found for the yield of condensates, while relevant deviations in the yield of char are found for all materials other than wheat straw. The yield of aqueous condensate is underestimated for all materials other than wheat straw, while the production of gas is not noticeably higher. This indicates a clear influence of the reaction networks, which decision was based on modeling wheat straw as best as possible. The production of first condensate is always underestimated, due to an overestimated volatility, as discussed during the

analysis of Figure *3*. These results contrast very clearly with those obtained by [91]Fonseca [91], in which the flow rate of both condensates were defined a priori based on experimental mass balances.

Not only is the product distribution relevant for further comparison, but also the condensate composition, which is presented in Figure 5. Deviations are particularly noticeable in all groups besides water, due not only lower production of these species in the modeled pyrolysis reactions compared to experimental data, but also due to influence of the liquid-vapor modeling. The latter is very noticeable for water and acids, due to their volatility at first condensation conditions, that leads to a higher evaporation rate than what is observed in the volatilization setup.

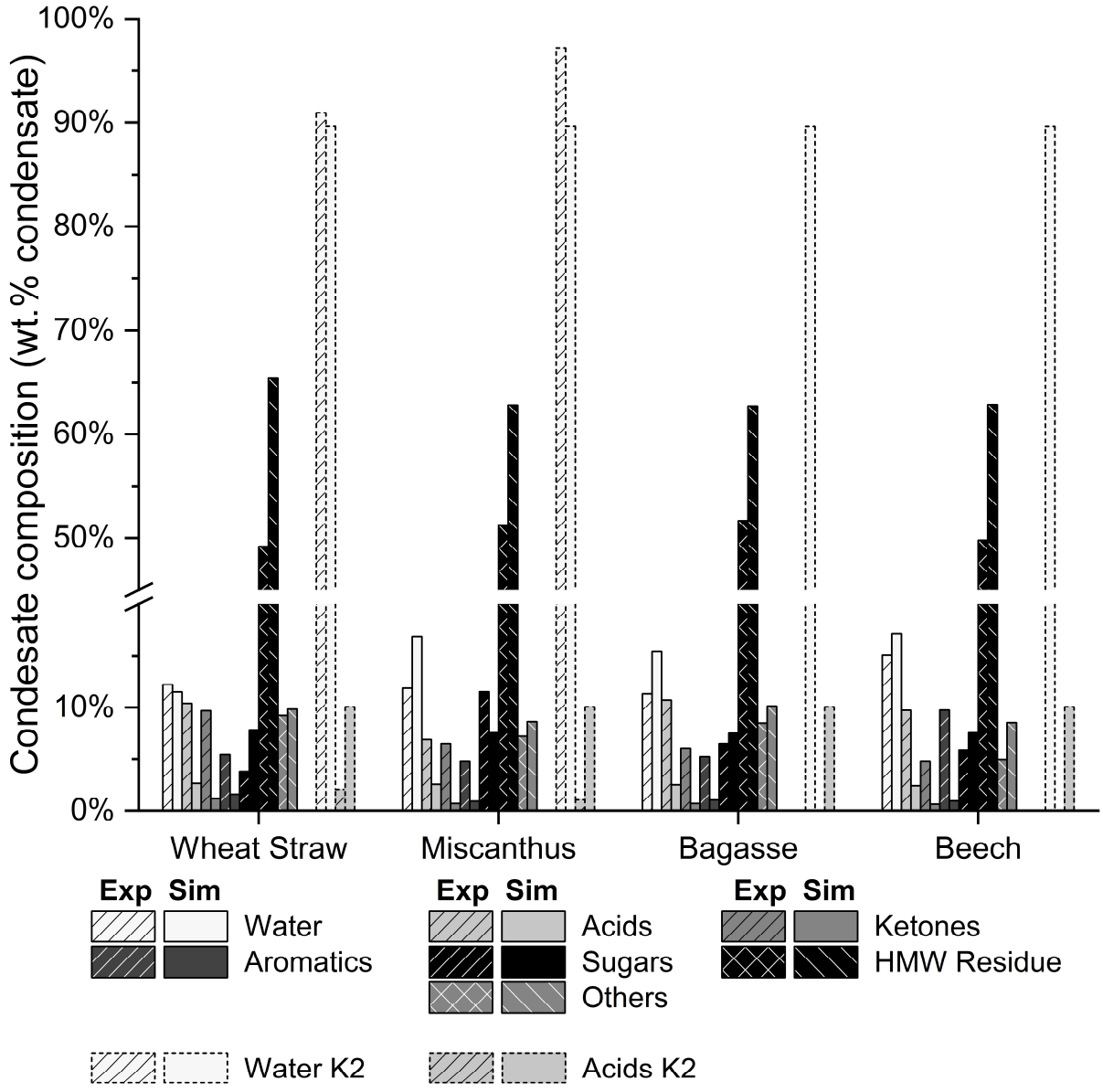

Figure 5: Comparison of condensate composition between experimental and simulated results. Values in K2 refer to the second condensate. Experimental data sourced from the internal database in IKFT-KIT. Deficit calculated assuming a difference to 360 kg/h.

Focused mostly on the reactor model, it is relevant to estimate the heat demand of the pyrolysis process. Several authors have provided estimates of ranges for this value for different biomass feedstocks and process conditions, and a good collection of these values has been compiled by Ábrego et al. [92], and discuss the notorious effect of the particle size and the measurement technique on the variability of this demand. Henrich et al. [82] estimated this value for several

feedstocks using similar equipment to the one employed to obtain the experimental data used in this work. It is also relevant to discuss whether this heat demand could be supplied by the combustion of pyrolysis gas, a material of low economic relevance, and a fraction the produced pyrolysis char, following the logic employed by Fonseca et al. [7]. These values can be found in Table 4.

Table 4: Estimated heat demand of the reactor estimated using different methods, compared to the heat potential of pyrolysis gas and coke. Provided is an estimated of the fraction of coke necessary to supply the estimated heat demand after using the pyrolysis gas for this propose.

	Heat demand of reactor					**Heat supply**		
	This work	Henrich et al. [82]	Fonseca et al. [7]	Polin et al. [84]	Zheng et al. [85]	Gas (this work)	Coke (this work)	% coke needed
Wheat Straw	168	143	133	75-116	116-306	112	370	15%
Miscanthus	137	-	-		-	121	322	5%
Bagasse	430	-	-		-	121	501	62%
Beech	213	150	-		-	127	298	29%

The results in Table 4 cast light on the effect of small differences in feedstock composition in the estimation of the heat demand, and show clear shortcomings of these models in handling differences in ash, moisture and lignocellulosic content and providing more realistic results. Compared to the results presented in Table 2 and Table 3, the results differ due to the definition of secondary pyrolysis reactions. Fonseca [91] observed similar issues when applying a similar model predict the heat demand of wheat straw conditioned to different moisture contents, and observed an unrealistic value for very low moisture contents, thus casting doubts on the viability of the results observed for bagasse and beech wood. As seen during the discussion of Figure 4, the most deviant results are the ones in which either ash or moisture content deviate the furthest from wheat straw (Table S 1 in the SI).

Conclusions

In the expansive domain of biomass conversion, fast pyrolysis is a widely studied process for the energetic valorization of solid feedstocks. Despite this attention, the scarcity of robust models capable of predicting product distribution and provide fully characterized products is notorious. The model presented in this work attempts to address prevalent deficiencies in existing models, providing an alternative of increased predictive ability.

The simulation of fast pyrolysis undertaken in this study has delved into the intricacies of secondary pyrolysis phenomena, by selecting reaction mechanisms and kinetics that can bridge the gap between primary pyrolysis products and real pyrolysis product composition. Although aging phenomena, a significant consideration, remained outside the scope of this work, the focus on secondary pyrolysis enriches our understanding without disregarding the complexities associated with aging.

Integral to our approach is the incorporation of rigorously modeled condensation loops, anchored around scrubbing columns that utilize pyrolysis condensates as quenching media for incoming hot vapor. Challenges pertaining to loop initialization, preserving the model's predictive prowess, and decisions regarding the thermodynamic model for liquid-vapor equilibria are thoroughly addressed. However, it is important to note that the use of reaction networks, employing a simplified set of

possible products, results in distinct equilibria behavior compared to real processes, showcasing higher vaporization and lower condensate recovery. Moreover, the nature of the high molecular weight residue, which influence on the proper modeling of equilibria during product separation had been made evident by Ille et al. [53], is considered in a fully-characterized surrogate molecule, designed based on experimental characterization of water-insoluble pyrolysis residua. [91]

The complex methodology employed in the study did not necessarily yield favorable outcomes, as several limitations of the model became evident during the validation phase. While the product distribution presented overall low deviations when compared to the experimental values (under 12 wt.%), the models presented a poor estimation of the condensate flow rates and compositions, as well as heat demand, a factor more pronounced when applied to biomass types beyond the calibration biomass (wheat straw). In this case, it is impossible to know if the effects of the ash content of the feedstock in the yields and compositions of the different phases are reflected in the results of the model. Moreover, the occurrence of phenomena like aging are not considered in the context of this paper [80]. These shortcomings underscore the need for continued research and refinement in order to enhance the predictive capabilities of the model across a broader range of biomasses.

Nonetheless, the presence of a more complex condensation system and the full characterization of the HMWR are relevant vantage points when comparing to more establish pyrolysis models, which do not reflect this bio-oil complexity, or sacrifice predictive capacity and flexibility by employing black box reactor models or gas-phase focused reaction models (see Table 1). Comparison of estimated and experimental bio-oil compositions are also frequently not performed in literature about Aspen Plus® models of biomass pyrolysis.

In light of the challenges identified, this work not only contributes valuable insights into the simulation of fast pyrolysis but also highlights avenues for future investigation and improvement. As we strive for greater accuracy and applicability in modeling pyrolysis processes, addressing these limitations will be essential for advancing our understanding and facilitating the development of more robust and versatile simulation tools in the field.

References

[1] P. Basu, Biomass Gasification and Pyrolysis: Practical Design and Theory, Elsevier, 2010.

[2] M. Tripathi, J.N. Sahu, P. Ganesan, Effect of process parameters on production of biochar from biomass waste through pyrolysis: A review, Renewable and Sustainable Energy Reviews. 55 (2016) 467–481. https://doi.org/10.1016/j.rser.2015.10.122.

[3] A.V. V. Bridgwater, Review of fast pyrolysis of biomass and product upgrading, Biomass Bioenergy. 38 (2012) 68–94. https://doi.org/10.1016/j.biombioe.2011.01.048.

[4] A. Demirbas, G. Arin, An Overview of Biomass Pyrolysis, Energy Sources. 24 (2002) 471–482. https://doi.org/10.1080/00908310252889979.

[5] N. Weih, A. Funke, Y. Ille, C. Pfitzer, A. Niebel, N. Dahmen, Online Balancing of a Pilot Scale Fast Pyrolysis Plant, in: European Biomass Conference and Exhibition Proceedings, 2017.

[6] F.G. Fonseca, A. Funke, A. Niebel, A.P.S. Dias, N. Dahmen, Moisture content as a design and operational parameter for fast pyrolysis, in: 1. Deutsches Doktorandenkolloquium Bioenergie, DBFZ Deutsches Biomasseforschungszentrum gemeinnützige GmbH, 2018: p. 286.

[7] F.G. Fonseca, A. Funke, A. Niebel, A.P. Soares Dias, N. Dahmen, Moisture content as a design and operational parameter for fast pyrolysis, J Anal Appl Pyrolysis. 139 (2019) 73–86. https://doi.org/10.1016/j.jaap.2019.01.012.

[8] M. Van de Velden, J. Baeyens, A. Brems, B. Janssens, R. Dewil, Fundamentals, kinetics and endothermicity of the biomass pyrolysis reaction, Renew Energy. 35 (2010) 232–242. https://doi.org/10.1016/j.renene.2009.04.019.

[9] C.C. Schmitt, F.G. Fonseca, M.M.C. Fraga, A. Wisniewski, S. Karp, Á.H. Mello José, R.C.L.B. Rodrigues, R. Moreira, D.E. Hirayama, K. Raffelt, N. Dahmen, A.W. Jr, S. Karp, Á. Henrique, M. José, C. Rita, R. Moreira, D. Eiji, K. Raffelt, N. Dahmen, Thermochemical and Catalytic Conversion Technologies for the Development of Brazilian Biomass Utilization, Catalysts. 11 (2021) 1549. https://doi.org/10.3390/catal11121549.

[10] A.V. Bridgwater, Renewable fuels and chemicals by thermal processing of biomass, Chemical Engineering Journal. 91 (2003) 87–102. https://doi.org/10.1016/S1385-8947(02)00142-0.

[11] Honeywell UOP, RTP Biomass Conversion - Renewable Fuels, (n.d.). https://uop.honeywell.com/en/industry-solutions/renewable-fuels/rtp-biomass-conversion (accessed May 19, 2021).

[12] A. Krutof, K.A. Hawboldt, Upgrading of biomass sourced pyrolysis oil review: focus on co-pyrolysis and vapour upgrading during pyrolysis, Biomass Convers Biorefin. 8 (2018) 775–787. https://doi.org/10.1007/s13399-018-0326-6.

[13] A. Krutof, K. Hawboldt, Blends of pyrolysis oil, petroleum, and other bio-based fuels: A review, Renewable and Sustainable Energy Reviews. 59 (2016) 406–419. https://doi.org/10.1016/j.rser.2015.12.304.

[14] C. Pfitzer, N. Dahmen, N. Tröger, F. Weirich, J. Sauer, A. Günther, M. Müller-Hagedorn, Fast Pyrolysis of Wheat Straw in the Bioliq Pilot Plant, Energy and Fuels. 30 (2016) 8047–8054. https://doi.org/10.1021/acs.energyfuels.6b01412.

[15] C.E. Pfitzer, N. Dahmen, N. Tröger, F. Weirich, J. Sauer, First Results of the Bioliq ® Fast Pyrolysis Pilot Plant, in: 22nd European Biomass Conference and Exhibition, 2014. https://doi.org/10.5071/22ndEUBCE2014-3CV.2.70.

[16] F. Trippe, M. Fröhling, F. Schultmann, R. Stahl, E. Henrich, Techno-economic analysis of fast pyrolysis as a process step within biomass-to-liquid fuel production, Waste Biomass Valorization. 1 (2010) 415–430. https://doi.org/10.1007/s12649-010-9039-1.

[17] A. Niebel, A. Funke, C. Pfitzer, N. Dahmen, N. Weih, D. Richter, B. Zimmerlin, Fast Pyrolysis of Wheat Straw—Improvements of Operational Stability in 10 Years of Bioliq Pilot Plant Operation, Energy & Fuels. 35 (2021) 11333–11345. https://doi.org/10.1021/acs.energyfuels.1c00851.

[18] A.S.N. Mahmood, J.G. Brammer, A. Hornung, A. Steele, S. Poulston, The intermediate pyrolysis and catalytic steam reforming of Brewers spent grain, J Anal Appl Pyrolysis. 103 (2013) 328–342. https://doi.org/10.1016/j.jaap.2012.09.009.

[19] R.J. Evans, T.A. Milne, Molecular characterization of the pyrolysis of biomass, Energy & Fuels. 1 (1987) 123–137. https://doi.org/10.1021/ef00002a001.

[20] E. Ranzi, P.E.A. Debiagi, A. Frassoldati, Mathematical Modeling of Fast Biomass Pyrolysis and Bio-Oil Formation. Note II: Secondary Gas-Phase Reactions and Bio-Oil Formation, ACS Sustain Chem Eng. 5 (2017) 2882–2896. https://doi.org/10.1021/acssuschemeng.6b03098.

[21] R.S. Miller, J. Bellan, A generalized biomass pyrolysis model based on superimposed cellulose, hemicellulose and lignin kinetics, Combustion Science and Technology. 126 (1997) 97–137. https://doi.org/10.1080/00102209708935670.

[22] J. Montoya, B. Pecha, F.C. Janna, M. Garcia-Perez, Single particle model for biomass pyrolysis with bubble formation dynamics inside the liquid intermediate and its contribution to aerosol formation by thermal ejection, J Anal Appl Pyrolysis. 124 (2017) 204–218. https://doi.org/10.1016/j.jaap.2017.02.004.

[23] D. Humbird, A. Trendewicz, R. Braun, A. Dutta, One-Dimensional Biomass Fast Pyrolysis Model with Reaction Kinetics Integrated in an Aspen Plus Biorefinery Process Model, ACS Sustain Chem Eng. 5 (2017) 2463–2470. https://doi.org/10.1021/acssuschemeng.6b02809.

[24] M. Carrier, M. Windt, B. Ziegler, J. Appelt, B. Saake, D. Meier, A. Bridgwater, Quantitative Insights into the Fast Pyrolysis of Extracted Cellulose, Hemicelluloses, and Lignin, ChemSusChem. 10 (2017) 3212–3224. https://doi.org/10.1002/cssc.201700984.

[25] J. Ward, M.G.G. Rasul, M.M.K.M.K. Bhuiya, Energy Recovery from Biomass by Fast Pyrolysis, Procedia Eng. 90 (2014) 669–674. https://doi.org/10.1016/j.proeng.2014.11.791.

[26] K. Onarheim, Y.Y. Solantausta, J. Lehto, Process Simulation Development of Fast Pyrolysis of Wood Using Aspen Plus, Energy & Fuels. 29 (2015) 205–217. https://doi.org/10.1021/ef502023y.

[27] E. Ranzi, A. Cuoci, T. Faravelli, A. Frassoldati, G. Migliavacca, S. Pierucci, S. Sommariva, Chemical Kinetics of Biomass Pyrolysis, Energ Fuel. 22 (2008) 4292–4300. https://doi.org/10.1021/ef800551t.

[28] B. Scholze, C. Hanser, D. Meier, Characterization of the water-insoluble fraction from fast pyrolysis liquids (pyrolytic lignin): Part II. GPC, carbonyl goups, and 13C-NMR, J Anal Appl Pyrolysis. 58–59 (2001) 387–400. https://doi.org/10.1016/S0165-2370(00)00173-X.

[29] J.F. Peters, S.W. Banks, A. V. Bridgwater, J. Dufour, A kinetic reaction model for biomass pyrolysis processes in Aspen Plus, Appl Energy. 188 (2017) 595–603. https://doi.org/10.1016/j.apenergy.2016.12.030.

[30] M. Corbetta, S. Pierucci, E. Ranzi, H. Bennadji, E.M. Fisher, Multistep Kinetic Model of Biomass Pyrolysis, in: XXXVI Meeting of the Italian Section of the Combustion Institute, 2013: pp. 4–9.

[31] E. Ranzi, M. Corbetta, F. Manenti, S. Pierucci, Kinetic modeling of the thermal degradation and combustion of biomass, Chem Eng Sci. 110 (2014) 2–12. https://doi.org/10.1016/j.ces.2013.08.014.

[32] E. Ranzi, P.E.A. Debiagi, A. Frassoldati, Mathematical Modeling of Fast Biomass Pyrolysis and Bio-Oil Formation. Note I: Kinetic Mechanism of Biomass Pyrolysis, ACS Sustain Chem Eng. 5 (2017) 2867–2881. https://doi.org/10.1021/acssuschemeng.6b03096.

[33] P.E.A. Debiagi, C. Pecchi, G. Gentile, A. Frassoldati, A. Cuoci, T. Faravelli, E. Ranzi, Extractives Extend the Applicability of Multistep Kinetic Scheme of Biomass Pyrolysis, Energy & Fuels. 29 (2015) 6544–6555. https://doi.org/10.1021/acs.energyfuels.5b01753.

[34] M. Corbetta, A. Frassoldati, H. Bennadji, K. Smith, M.J. Serapiglia, G. Gauthier, T. Melkior, E. Ranzi, E.M. Fisher, Pyrolysis of Centimeter-Scale Woody Biomass Particles: Kinetic Modeling and Experimental Validation, Energy & Fuels. 28 (2014) 3884–3898. https://doi.org/10.1021/ef500525v.

[35] A. Anca-Couce, R. Mehrabian, R. Scharler, I. Obernberger, Kinetic scheme of biomass pyrolysis considering secondary charring reactions, Energy Convers Manag. 87 (2014) 687–696. https://doi.org/10.1016/j.enconman.2014.07.061.

[36] A. Anca-Couce, R. Scharler, Modelling heat of reaction in biomass pyrolysis with detailed reaction schemes, Fuel. 206 (2017) 572–579. https://doi.org/10.1016/j.fuel.2017.06.011.

[37] A. Trendewicz, R. Evans, A. Dutta, R. Sykes, D. Carpenter, R. Braun, Evaluating the effect of potassium on cellulose pyrolysis reaction kinetics, Biomass Bioenergy. 74 (2015) 15–25. https://doi.org/10.1016/j.biombioe.2015.01.001.

[38] F.G. Fonseca, A. Anca-Couce, A. Funke, N. Dahmen, Challenges in kinetic parameter determination for wheat straw pyrolysis, Energies (Basel). 15 (2022) 7240. https://doi.org/doi.org/10.3390/en15197240.

[39] G. Kabir, B.H. Hameed, Recent progress on catalytic pyrolysis of lignocellulosic biomass to high-grade bio-oil and bio-chemicals, Renewable and Sustainable Energy Reviews. 70 (2017) 945–967. https://doi.org/10.1016/j.rser.2016.12.001.

[40] P. Lestinsky, A. Palit, Wood Pyrolysis Using Aspen Plus Simulation and Industrially Applicable Model, GeoScience Engineering. 62 (2016) 11–16. https://doi.org/10.1515/gse-2016-0003.

[41] A. Visconti, M. Miccio, C. Republic, D. Juchelková, Equilibrium-based simulation of lignocellulosic biomass pyrolysis via Aspen Plus ®, in: Recent Advances in Applied Mathematics, Modelling and Simulation, 2014.

[42] I.Y. Mohammed, Y.A. Abakr, R. Mokaya, Integrated biomass thermochemical conversion for clean energy production: Process design and economic analysis, J Environ Chem Eng. 7 (2019) 103093. https://doi.org/10.1016/j.jece.2019.103093.

[43] R.J. Wooley, V. Putsche, Development of an ASPEN PLUS physical property database for biofuels components, Golden, Colorado, 1996. https://doi.org/10.2172/257362.

[44] M.B. Gorensek, R. Shukre, C.-C.C. Chen, Development of a Thermophysical Properties Model for Flowsheet Simulation of Biomass Pyrolysis Processes, ACS Sustain Chem Eng. 7 (2019) 9017–9027. https://doi.org/10.1021/acssuschemeng.9b01278.

[45] R. Demol, A. Dufour, Y. Rogaume, G. Mauviel, Production of Purified H_2, Heat, and Biochar from Wood: Comparison between Gasification and Autothermal Pyrolysis Based on Advanced Process Modeling, Energy & Fuels. 36 (2022) 488–501. https://doi.org/10.1021/acs.energyfuels.1c03528.

[46] N.L. Hammer, A. a Boateng, C. a Mullen, M.C. Wheeler, Aspen Plus®and economic modeling of equine waste utilization for localized hot water heating via fast pyrolysis., J Environ Manage. 128 (2013) 594–601. https://doi.org/10.1016/j.jenvman.2013.06.008.

[47] A. Oasmaa, I. Fonts, M.R. Pelaez-Samaniego, M.E.M. Garcia-Perez, M.E.M. Garcia-Perez, Pyrolysis Oil Multiphase Behavior and Phase Stability: A Review, Energy and Fuels. 30 (2016) 6179–6200. https://doi.org/10.1021/acs.energyfuels.6b01287.

[48] J.C. del Río, J. Rencoret, P. Prinsen, Á.T. Martínez, J. Ralph, A. Gutiérrez, Structural Characterization of Wheat Straw Lignin as Revealed by Analytical Pyrolysis, 2D-NMR, and Reductive Cleavage Methods, J Agric Food Chem. 60 (2012) 5922–5935. https://doi.org/10.1021/jf301002n.

[49] R. Bayerbach, D. Meier, Characterization of the water-insoluble fraction from fast pyrolysis liquids (pyrolytic lignin). Part IV: Structure elucidation of oligomeric molecules, J Anal Appl Pyrolysis. 85 (2009) 98–107. https://doi.org/10.1016/j.jaap.2008.10.021.

[50] A.U. Şen, F.G. Fonseca, A. Funke, H. Pereira, F. Lemos, Pyrolysis kinetics and estimation of chemical composition of Quercus cerris cork, Biomass Convers Biorefin. (2020). https://doi.org/10.1007/s13399-020-00964-y.

[51] C. Gustavsson, L. Nilsson, Co-production of pyrolysis oil in district heating plants: Systems analysis of dual fluidized-bed pyrolysis with sequential vapor condensation, Energy and Fuels. 27 (2013) 5313–5319. https://doi.org/10.1021/ef401143v.

[52] D.C. Elliott, D. Meier, A. Oasmaa, B. Van De Beld, A. V. Bridgwater, M. Marklund, Results of the International Energy Agency Round Robin on Fast Pyrolysis Bio-oil Production, Energy and Fuels. 31 (2017) 5111–5119. https://doi.org/10.1021/acs.energyfuels.6b03502.

[53] Y. Ille, F. Kröhl, A. Velez, A. Funke, S. Pereda, K. Schaber, N. Dahmen, Activity of water in pyrolysis oil—Experiments and modelling, J Anal Appl Pyrolysis. 135 (2018) 260–270. https://doi.org/10.1016/j.jaap.2018.08.027.

[54] M. Fortin, M. Mohadjer Beromi, A. Lai, P.C. Tarves, C.A. Mullen, A.A. Boateng, N.M. West, Structural Analysis of Pyrolytic Lignins Isolated from Switchgrass Fast-Pyrolysis Oil, Energy & Fuels. 29 (2015) 8017–8026. https://doi.org/10.1021/acs.energyfuels.5b01726.

[55] A.P. Pinheiro Pires, J. Arauzo, I. Fonts, M.E. Domine, A. Fernández Arroyo, M.E.M.M.E. Garcia-Perez, J. Montoya, F. Chejne, P. Pfromm, M.E.M.M.E. Garcia-Perez, Challenges and opportunities for bio-oil refining: A review, Energy and Fuels. 33 (2019) 4683–4720. https://doi.org/10.1021/acs.energyfuels.9b00039.

[56] I. Fonts, M. Atienza-Martínez, H.-H.H. Carstensen, M. Benés, A.P. Pinheiro Pires, M. Garcia-Perez, R. Bilbao, Thermodynamic and Physical Property Estimation of Compounds Derived from the Fast Pyrolysis of Lignocellulosic Materials, Energy & Fuels. 35 (2021) 17114–17137. https://doi.org/10.1021/acs.energyfuels.1c01709.

[57] F. Kröhl, Berechnung der Aktivitätskoefizienten einer Modellmischung fur Pyrolyseöle mittels Gruppenbeitragsmethoden, Bachelorarbeit, Karlsruhe Institute für Technologie, 2015.

[58] C. Perez Locas, V.A. Yaylayan, Isotope Labeling Studies on the Formation of 5-(Hydroxymethyl)-2-furaldehyde (HMF) from Sucrose by Pyrolysis-GC/MS, J Agric Food Chem. 56 (2008) 6717–6723. https://doi.org/10.1021/jf8010245.

[59] X. Zhang, W. Yang, W. Blasiak, Thermal decomposition mechanism of levoglucosan during cellulose pyrolysis, J Anal Appl Pyrolysis. 96 (2012) 110–119. https://doi.org/10.1016/j.jaap.2012.03.012.

[60] A.D. Pouwels, G.B. Eijkel, J.J. Boon, Curie-point pyrolysis-capillary gas chromatography-high-resolution mass spectrometry of microcrystalline cellulose, J Anal Appl Pyrolysis. 14 (1989) 237–280. https://doi.org/10.1016/0165-2370(89)80003-8.

[61] T. Hosoya, H. Kawamoto, S. Saka, Different pyrolytic pathways of levoglucosan in vapor- and liquid/solid-phases, J Anal Appl Pyrolysis. 83 (2008) 64–70. https://doi.org/10.1016/j.jaap.2008.06.008.

[62] P.Y. Nikolov, V.A. Yaylayan, Thermal Decomposition of 5-(Hydroxymethyl)-2-furaldehyde (HMF) and Its Further Transformations in the Presence of Glycine, J Agric Food Chem. 59 (2011) 10104–10113. https://doi.org/10.1021/jf202470u.

[63] E.-J. Shin, M.R. Nimlos, R.J. Evans, Kinetic analysis of the gas-phase pyrolysis of carbohydrates, Fuel. 80 (2001) 1697–1709. https://doi.org/10.1016/S0016-2361(01)00056-4.

[64] A.K. Vasiliou, J.H. Kim, T.K. Ormond, K.M. Piech, K.N. Urness, A.M. Scheer, D.J. Robichaud, C. Mukarakate, M.R. Nimlos, J.W. Daily, Q. Guan, H.-H. Carstensen, G.B. Ellison, Biomass pyrolysis: Thermal decomposition mechanisms of furfural and benzaldehyde, J Chem Phys. 139 (2013) 104310. https://doi.org/10.1063/1.4819788.

[65] M.A. Grela, A.J. Colussi, Kinetics and mechanism of the thermal decomposition of unsaturated aldehydes: benzaldehyde, 2-butenal, and 2-furaldehyde, J Phys Chem. 90 (1986) 434–437. https://doi.org/10.1021/j100275a016.

[66] B. Girisuta, L.P.B.M. Janssen, H.J. Heeres, A kinetic study on the decomposition of 5-hydroxymethylfurfural into levulinic acid, Green Chemistry. 8 (2006) 701. https://doi.org/10.1039/b518176c.

[67] W. Chen, H. Hu, Q. Cai, S. Zhang, Synergistic Effects of Furfural and Sulfuric Acid on the Decomposition of Levulinic Acid, Energy & Fuels. 34 (2020) 2238–2245. https://doi.org/10.1021/acs.energyfuels.9b03971.

[68] F. Shafizadeh, G.D. McGinnis, C.W. Philpot, Thermal degradation of xylan and related model compounds, Carbohydr Res. 25 (1972) 23–33. https://doi.org/10.1016/S0008-6215(00)82742-1.

[69] S. Wang, B. Ru, H. Lin, Z. Luo, Degradation mechanism of monosaccharides and xylan under pyrolytic conditions with theoretic modeling on the energy profiles, Bioresour Technol. 143 (2013) 378–383. https://doi.org/10.1016/j.biortech.2013.06.026.

[70] U. Räisänen, I. Pitkänen, H. Halttunen, M. Hurtta, Formation of the main degradation compounds from arabinose, xylose, mannose and arabinitol during pyrolysis, J Therm Anal Calorim. 72 (2003) 481–488. https://doi.org/10.1023/A:1024557011975.

[71] A.E. Harman-Ware, M. Crocker, A.P. Kaur, M.S. Meier, D. Kato, B. Lynn, Pyrolysis–GC/MS of sinapyl and coniferyl alcohol, J Anal Appl Pyrolysis. 99 (2013) 161–169. https://doi.org/10.1016/j.jaap.2012.10.001.

[72] R.C. Neves, A. Funke, E. Olivarez-Gómez, A. Bonomia, N. Dahmen, R. Maciel Filho, Process simulation of fast pyrolysis to produce bioslurry from lignocellulosic biomass residues combining first and second generation biofuels, in: 6th International Symposium on Energy from Biomass and Waste, Venice, Italy, 2016.

[73] Y.C. Ardila, Gaseificação da biomassa para a produção de gás de síntese e posterior fermentação para bioetanol : modelagem e simulação do processo, PhD, Universidade Estadual de Campinas, 2015. http://repositorio.unicamp.br/jspui/handle/REPOSIP/266052.

[74] J.P.P. Diebold, A Review of the Chemical and Physical Mechanisms of the Storage Stability of Fast Pyrolysis Bio-Oils, Lakewood, CO, USA, 2000. https://doi.org/NREL/SR-570-27613.

[75] S.W. Banks, D.J. Nowakowski, A. V. Bridgwater, Impact of Potassium and Phosphorus in Biomass on the Properties of Fast Pyrolysis Bio-oil, Energy & Fuels. 30 (2016) 8009–8018. https://doi.org/10.1021/acs.energyfuels.6b01044.

[76] J. Cai, Md.M. Rahman, S. Zhang, M. Sarker, X. Zhang, Y. Zhang, X. Yu, E.H. Fini, Review on Aging of Bio-Oil from Biomass Pyrolysis and Strategy to Slowing Aging, Energy & Fuels. 35 (2021) 11665–11692. https://doi.org/10.1021/acs.energyfuels.1c01214.

[77] A. Oasmaa, K. Sipilä, Y. Solantausta, E. Kuoppala, Quality Improvement of Pyrolysis Liquid: Effect of Light Volatiles on the Stability of Pyrolysis Liquids, Energy & Fuels. 19 (2005) 2556–2561. https://doi.org/10.1021/ef0400924.

[78] Q. Zhang, L. Zhang, T. Wang, Y. Xu, Q. Zhang, L. Ma, M. He, K. Li, Upgrading of Bio-oil by Removing Carboxylic Acids in Supercritical Ethanol, Energy Procedia. 61 (2014) 1033–1036. https://doi.org/10.1016/j.egypro.2014.11.1018.

[79] R. Wang, H. Ben, Accelerated Aging Process of Bio-Oil Model Compounds: A Mechanism Study, Front Energy Res. 8 (2020). https://doi.org/10.3389/fenrg.2020.00079.

[80] S. Black, J.R. Ferrell, Accelerated aging of fast pyrolysis bio-oil: a new method based on carbonyl titration, RSC Adv. 10 (2020) 10046–10054. https://doi.org/10.1039/D0RA00046A.

[81] R.J.M. Westerhof, N.J.M. Kuipers, S.R.A. Kersten, W.P.M. van Swaaij, Controlling the water content of biomass fast pyrolysis oil, Ind Eng Chem Res. 46 (2007) 9238–9247. https://doi.org/10.1021/ie070684k.

[82] E. Henrich, N. Dahmen, F. Weirich, R. Reimert, C. Kornmayer, Fast pyrolysis of lignocellulosics in a twin screw mixer reactor, Fuel Processing Technology. 143 (2016) 151–161. https://doi.org/10.1016/j.fuproc.2015.11.003.

[83] Aspen Technology Inc., Aspen Physical Property System: Physical Property Methods, (2016).

[84] J.P. Polin, C.A. Peterson, L.E. Whitmer, R.G. Smith, R.C. Brown, Process intensification of biomass fast pyrolysis through autothermal operation of a fluidized bed reactor, Appl Energy. 249 (2019) 276–285. https://doi.org/10.1016/j.apenergy.2019.04.154.

[85] X. Zheng, Z. Zhong, B. Zhang, H. Du, W. Wang, Q. Li, Environmental impact comparison of wheat straw fast pyrolysis systems with different hydrogen production processes based on life cycle assessment, Waste Management & Research: The Journal for a Sustainable Circular Economy. 40 (2022) 654–664. https://doi.org/10.1177/0734242X211045004.

[86] H. Yang, S. Kudo, H.-P. Kuo, K. Norinaga, A. Mori, O. Mašek, J. Hayashi, Estimation of Enthalpy of Bio-Oil Vapor and Heat Required for Pyrolysis of Biomass, Energy & Fuels. 27 (2013) 2675–2686. https://doi.org/10.1021/ef400199z.

[87] R. Grandl, Simulation der Stoff- und Wärmetransportvorgänge bei der Schnellpyrolyse von Lignocellulose im Doppelschneckenmischreaktor, 2022. https://swb.bsz-bw.de/DB=2.1/PPN?PPN=1817012479.

[88] W. Peters, Schnellentgasung von Steinkohlen, 1963. https://swb.bsz-bw.de/DB=2.1/PPN?PPN=1167585291.

[89] Y. Qiao, B. Wang, P. Zong, Y. Tian, F. Xu, D. Li, F. Li, Y. Tian, Thermal behavior, kinetics and fast pyrolysis characteristics of palm oil: Analytical TG-FTIR and Py-GC/MS study, Energy Convers Manag. 199 (2019) 111964. https://doi.org/10.1016/j.enconman.2019.111964.

[90] J. Asomaning, P. Mussone, D.C. Bressler, Pyrolysis of polyunsaturated fatty acids, Fuel Processing Technology. 120 (2014) 89–95. https://doi.org/10.1016/j.fuproc.2013.12.007.

[91] F.G. Fonseca, Process simulation and optimization of biomass fast pyrolysis, Ph.D, Karlsruhe Institute of Technology, 2023. https://doi.org/10.5445/IR/1000161174.

[92] J. Ábrego, M. Atienza-Martínez, F. Plou, J. Arauzo, Heat requirement for fixed bed pyrolysis of beechwood chips, Energy. 178 (2019) 145–157. https://doi.org/10.1016/j.energy.2019.04.078.